

High energy anomaly dichotomy in electron- and hole-doped high T_c superconductors

B. Moritz¹, F. Schmitt^{1,2}, W. Meevasana^{1,3}, S. Johnston^{1,4}, E. M. Motoyama^{1,3}, M. Greven^{1,2,5}, D. H. Lu^{1,5}, C. Kim⁶, R. T. Scalettar⁷, Z.-X. Shen^{1,2,3,5}, and T. P. Devereaux¹

¹ *Stanford Institute for Materials and Energy Sciences,*

Stanford Linear Accelerator Center and Stanford University, Stanford, CA 94305, USA

² *Department of Applied Physics, Stanford University, Stanford, CA 94305, USA*

³ *Department of Physics, Stanford University, Stanford, CA 94305, USA*

⁴ *Department of Physics and Astronomy, University of Waterloo, Waterloo, ON N2L 3G1, Canada*

⁵ *Stanford Synchrotron Radiation Laboratory, Stanford Linear Accelerator Center, Menlo Park, CA 94025, USA*

⁶ *Institute of Physics and Applied Physics, Yonsei University, Seoul 120-749, Korea and*

⁷ *Physics Department, University of California - Davis, Davis, CA 95616, USA*

(Dated: May 29, 2019)

New results are presented from angle-resolved photoemission spectroscopy on the electron-doped cuprate $\text{Nd}_{1.83}\text{Ce}_{0.17}\text{CuO}_4$ that show a high energy anomaly in the dispersion at $\sim 500 - 600$ meV, approximately twice the energy scale observed in the hole-doped high T_c superconductors. Model calculations of the single-band Hubbard Hamiltonian highlight significant differences in the electronic structure of electron- and hole-doped cuprates, specifically related to the formation of the anomaly. The results indicate that the anomaly demarcates a transition, or cross-over, from a quasi-particle band at low binding energies near the Fermi level to valence bands at higher binding energy, assumed to be of strong oxygen character.

PACS numbers: 74.72.-h, 79.60.-i, 74.25.Jb, 71.10.Fd

Over the last decade significant advancements have improved the momentum and energy resolution of angle-resolved photoemission spectroscopy (ARPES) [1] that provides access to the single-particle spectral function $A(\mathbf{k}, \omega)$. While a significant probe of electronic structure in general, such advancements in ARPES have had a profound impact on the study of strongly correlated materials. A series of high resolution ARPES experiments at binding energies up to $\sim 1 - 1.5$ eV, made possible by these advancements, has revealed the presence of a high energy anomaly (HEA) in the dispersion of high T_c superconductors [2, 3, 4, 5, 6, 7, 8, 9]. In hole-doped compounds the anomaly, at an energy ~ 300 meV, is universally present in different materials, doping values and phases. A similar feature also has been observed in the half-filled parent insulators [10]. A number of theories have been advanced to explain the presence of this anomaly including spin-charge separation [3], spin polarons [11], in-gap band-tails [12], photoemission matrix elements [7], coupling to spin fluctuations [6, 13, 14], phonons [4], or plasmons [15] and strong correlation or “Mott” physics [2, 16, 17, 18, 19]. In particular, it has been proposed that no HEA should be present in electron-doped cuprates [18].

In this Letter, new results from ARPES experiments on $\text{Nd}_{1.83}\text{Ce}_{0.17}\text{CuO}_4$ (NCCO) reveal the presence of a HEA in electron-doped high T_c superconductors. The energy scale is approximately twice that found in the hole-doped high T_c compounds. This discovery constrains the possible mechanisms for the anomaly, now universally observed in the cuprates. This Letter also presents results from quantum Monte Carlo calculations of the single-band Hubbard model, in both the electron- and

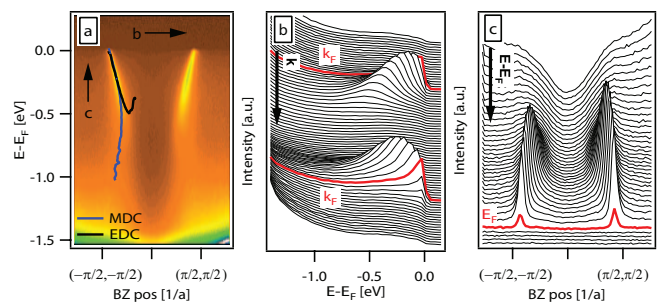


FIG. 1: (a) Intensity plot along a nodal cut in the first BZ of NCCO ($x=0.17$) taken at 16.75 eV incident energy. (b) Energy distribution curves (EDCs) and (c) momentum distribution curves (MDCs) of the cut in (a). The direction of the MDCs and EDCs are indicated by the black arrows in panel (a) and curves corresponding to k_f and E_f are highlighted in each panel. The HEA appears as a “waterfall” at an energy scale $\sim 500 - 600$ meV. (Color online.)

hole-doped regimes, indicating that the HEA can be connected to doping and subsequent spectral weight transfers into the lower/upper Hubbard band of p/n-type materials, respectively. These calculations reveal that the hole or electron doping is accompanied by the formation of a quasi-particle band at energies near E_f and that the HEA represents a cross-over from this band to valence bands at higher binding energies. In addition, the results highlight an electron/hole doping asymmetry in the HEA energy scale, in agreement with experiment.

The ARPES data were taken at beamline 5-4 of the Stanford Synchrotron Radiation Laboratory with a Scienta R4000 analyzer at a photon energy of 16.75 eV. The energy resolution was ~ 20 meV with an angular resolu-

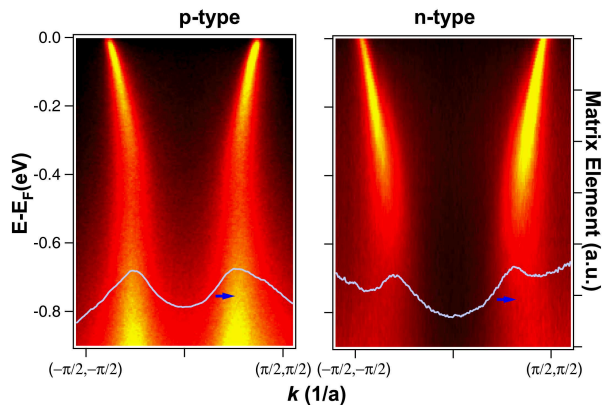


FIG. 2: Comparison of the HEA between hole- and electron-doped (p- and n-type) systems. The left panel shows the nodal ARPES data for BSCCO-2201 adapted from Ref. 2; the right panel shows the nodal data for NCCO. Matrix element profiles obtained from a 2D fitting procedure [20] are also shown in each panel. While the appearance of the HEA is affected by changes in the photoelectric matrix elements, they can not fully account for the anomaly itself. (Color online.)

tion $\sim 0.3^\circ$. NCCO single crystals were grown in 4 atm of oxygen using the traveling-solvent floating-zone technique, annealed for 10 h in argon at 970 C followed by 20 h in oxygen at 500 C and then cleaved and measured at 10 K and pressures better than 3×10^{-11} torr.

Figure 1 displays the ARPES data along a nodal cut $((-\pi/a, -\pi/a)$ to $(\pi/a, \pi/a)$) for NCCO. The intensity plot of Fig. 1(a) clearly shows the anomaly or “waterfall” in the dispersion at an energy $\sim 500 - 600$ meV. This is seen also in the energy distribution curves (EDCs) and the momentum distribution curves (MDCs) in Figs. 1(b) and (c), respectively. The EDC and MDC derived dispersions are superimposed over the intensity plot of Fig. 1(a). This HEA demarcates the transition between a quasi-particle band at low binding energy and the oxygen valence bands at energies $\gtrsim 1$ eV. While the MDCs appear to show a steep dispersion that bends back below the HEA, the EDCs show a shallower band with a bottom on the order of the HEA energy scale. This difference is similar to that found in the half-filled parent insulators [10] and hole-doped systems [3, 9].

A direct comparison of the ARPES data from $\text{Bi}_2\text{Sr}_2\text{CuO}_6$ (BSCCO-2201) [2] and NCCO is shown in Fig. 2. The HEAs are qualitatively similar in the two materials, but there are significant quantitative differences [2, 8]. Most importantly, for NCCO the HEA energy scale is approximately twice that found in the hole-doped materials and the main valence band weight also lies at higher binding energy.

To address the issues surrounding matrix elements that vary with incident photon energy, a 2D fitting procedure, described in Ref. 20, was used to extract the matrix elements along the nodal cut in both hole- and

electron-doped materials. The momentum space profiles are shown in Fig. 2. In particular, the matrix elements significantly reduce the ARPES intensity upon approaching the Γ -point. However, taken together with the EDC and MDC dispersions for these materials, the matrix elements affect the appearance of the HEA, but do not fully account for the effect.

The calculations presented in this Letter, focusing on the dichotomy between p-type and n-type materials, use the two-dimensional, single-band Hubbard Hamiltonian that serves as an effective, low energy model of the copper-oxide planes [21, 22] incorporating the effects of strong correlations. The single-band Hubbard Hamiltonian has the form

$$H = - \sum_{ij,\sigma} t_{ij} c_{i,\sigma}^\dagger c_{j,\sigma} - \mu \sum_i n_i + \sum_i U (n_{i,\uparrow} - \frac{1}{2})(n_{i,\downarrow} - \frac{1}{2}),$$

where $\{t_{ij}\}$ is a set of tight-binding parameters where only nearest-neighbor t and next-nearest-neighbor t' are different from zero, $c_{i,\sigma}^\dagger (c_{i,\sigma})$ creates (annihilates) an electron with spin σ at site i and $n_{i,\sigma} = c_{i,\sigma}^\dagger c_{i,\sigma}$ with $n_i = n_{i,\uparrow} + n_{i,\downarrow}$. The chemical potential μ controls the electron filling; and, in what follows, the Hubbard repulsion U is set equal to the noninteracting electron bandwidth $W = 8t$.

Here, the single-band Hubbard model is studied using the determinant quantum Monte Carlo technique [23, 24], an auxiliary-field method, to obtain the finite temperature, imaginary time propagator $G_{ij}(\tau)$ on a finite-size cluster with periodic boundary conditions. The details of the method can be found in Ref. 23. The finite-size, square clusters used in this study have linear dimension $N = 8$ implying a momentum space grid spacing of $\pi/4$. The imaginary time interval, partitioned into L “slices” of size $\Delta\tau = \beta/L$, runs from 0 to $\beta = 1/T$, the inverse temperature, and t serves as the energy unit of the problem. Unless otherwise noted $\Delta\tau = 1/16t$.

The maximum entropy method [25, 26] provides an effective means of obtaining the spectral function $A(\mathbf{K}, \omega)$ from the imaginary time data on the grid $\{\mathbf{K}\}$ in momentum space. Once $A(\mathbf{K}, \omega)$ has been obtained, the single-particle self-energy $\Sigma(\mathbf{K}, \omega)$ can be extracted using Dyson’s equation and the tight-binding bandstructure. Assuming a weak momentum dependence to the self-energy, an interpolation routine provides the value of $\Sigma(\mathbf{k}, \omega)$ at an arbitrary point \mathbf{k} in the BZ and Dyson’s equation can be employed once again to compute $A(\mathbf{k}, \omega)$ at that point.

Results from calculation of $A(\mathbf{k}, \omega)$ for the single-band Hubbard model are shown in Figs. 3(a)-(d). The single-particle spectral function is shown for a representative p-type system with parameters $t' = -0.3t$ and $\beta = 3/t$ at $\sim 14\%$ hole doping ($\mu = -2.5t$) in Figs. 3(a) and (b) while (c) and (d) show the results for a representative n-type system with parameters $t' = -0.2t$ and $\beta = 3/t$

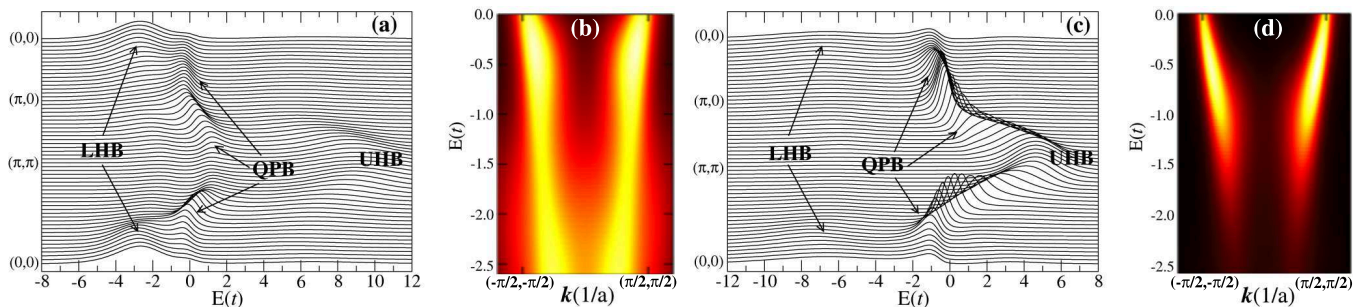


FIG. 3: Calculated single-particle spectral function $A(\mathbf{k}, \omega)$ for $\sim 14\%$ hole-doping ($\mu = -2.5t$, $t' = -0.3t$ and $\beta = 3/t$ in panels (a) and (b) and $\sim 16\%$ electron-doping ($\mu = 2.25t$, $t' = -0.2t$ and $\beta = 3/t$ in panels (c) and (d)). Panels (a) and (c) trace out the path $(0, 0) - (\pi, \pi) - (\pi, 0) - (0, 0)$ in the first BZ. Panels (b) and (d) focus on nodal cuts from $\sim (-\pi/2, -\pi/2)$ to $\sim (\pi/2, \pi/2)$ where representative photoelectric matrix elements have been used in creating the intensity plots. (Color online.)

at $\sim 16\%$ electron doping ($\mu = 2.25t$). For each system the tight-binding parameters and even Fermi surface topology are quite similar. However, note the two sets of parameters are not simply related by a particle-hole transformation and, in general, the experimentally determined bandstructure parameters would not reveal such a symmetry between hole- and electron-doped materials.

For the p-type system the lower Hubbard band (LHB) is essentially localized near the Γ -point with a weak tail of spectral intensity extending toward the points (π, π) and $(\pi, 0)$. The decrease in spectral weight in these tails approximately coincides with the location in momentum space identified with the HEA. The weak appearance of the upper Hubbard band (UHB) results from hole-doping [27, 28] as spectral weight is transferred into the LHB or more precisely the dispersive quasi-particle like band (QPB) that develops from low binding energy precursors found at half-filling [29]. These precursors resemble the low energy features seen in ARPES experiments on the parent insulator [10].

Along a nodal cut the QPB from the p-type calculation is highly dispersive crossing the Fermi level at $\sim (\pi/2, \pi/2)$. Near $(\pi/4, \pi/4)$ the spectral intensity in the band drops and the HEA appears as an apparent cross-over from the QPB to the LHB at an energy $\sim -0.5t$ to $-0.75t$, the HEA energy scale. While the spectral intensity decreases as the QPB approaches the Γ -point, the coexistence of the LHB and QPB over a significant momentum interval supports the cross-over scenario presented here.

In the n-type calculation, the dispersive QPB shown in Fig. 3(c) dips farther below the Fermi level than its p-type counterpart, to an energy $\sim -1.0t$ to $-1.5t$, in agreement with the results shown in Fig. 2. More importantly, the QPB arises from intermediate energy precursors in the UHB of the half-filled system [29], in contrast to the spectral weight forming the QPB in the p-type system. While there appears to be a weak tail of the UHB at significantly higher energies ($\sim 3t$ to $4t$), the dispersive feature and bulk of the UHB appear to meet

in another “waterfall” well above the Fermi level.

The appearance of the HEA as a “waterfall” at intermediate binding energies may be highlighted by applying photoelectric matrix elements, representative of experimentally derived values, to the results obtained from the calculations. Figures 3(b) and (d) show $A(\mathbf{k}, \omega)$ multiplied by these matrix elements (see Ref. 20) along a nodal cut for p-type and n-type systems, respectively. In each case the matrix elements severely suppress the intensity near the Γ -point. In particular for p-type systems, this behavior is consistent with the interpretation of the QPB as a renormalized Zhang-Rice singlet (ZRS) band with photoelectric matrix elements that also would reflect the robustness of the Zhang-Rice picture in different regions of the BZ [21, 30]. This suppression of intensity, particularly in the p-type calculation, leads to the appearance of the HEA as a “waterfall” due to the overlap of spectral weight at intermediate energies for \mathbf{k} away from the Γ -point. In the n-type calculation, the lack of significant spectral weight in the LHB leads to a simple suppression of intensity near the Γ -point without a significant overlap at intermediate energies. This result should be affected by the inclusion of additional valence band weight within multi-band treatments.

The relative spectral weight in the LHB and UHB as well as the HEA energy scale exemplify the dichotomy between p-type and n-type systems. A schematic of the band structure, confirmed by this study, can be found in Fig. 4. In a multi-band treatment incorporating planar oxygen degrees of freedom, the UHB and ZRS band correspond roughly to the UHB and LHB in the single-band Hubbard model. Additional bands (proper LHB, Zhang-Rice triplet and non-bonding oxygen) serve as marker states and play no role in the single-band calculations.

Upon hole doping in the single-band model, the chemical potential shifts into the LHB with a concomitant transfer of spectral weight from the UHB and increase in weight at energies near the chemical potential, forming the QPB. In contrast, upon electron doping, the chemical potential shifts into the UHB with a transfer of weight

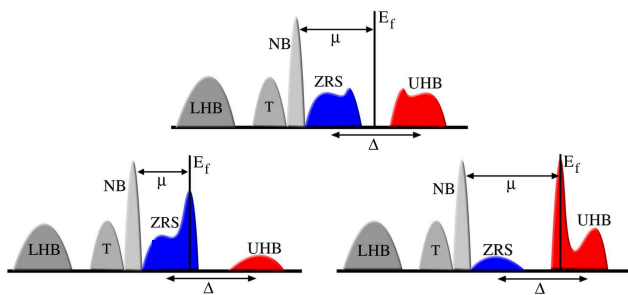


FIG. 4: Schematic diagram for the multiband structure of the copper-oxide plane highlighting the Zhang-Rice singlet (ZRS) band (blue) and upper Hubbard band (UHB) (red). The schematic also includes the lower Hubbard band (LHB), the Zhang-Rice triplet band (T) and the oxygen non-bonding band (NB). The ZRS band serves as the LHB in the single-band model. The chemical potential μ (Fermi level E_f) shifts as a function of hole or electron doping into the LHB (ZRS band) or the UHB, respectively. (Color online.)

to higher relative energy, again forming the bulk of the QPB in the n-type system. The chemical potential and spectral weight shifts with doping are consistent with the treatment presented in Ref. 27. Note with doping that the Mott gap does not simply collapse, but instead forms much of the intermediate energy regime below the HEA energy scale in the electron-doped calculation. This is in contrast to the hole-doped system in which the anomaly lies within the canonical LHB and the Mott gap has been effectively pushed above the Fermi level.

The results presented in this Letter support the conclusion that strong correlations and many body effects, here in the guise of the single-band Hubbard model, play a central role in the high energy anomaly. The calculations also echo some of the results of much earlier investigations into the spectral function of the single-band Hubbard model [29, 31, 32]. This study shows evidence for an anomaly in electron-doped materials and does not equate its energy scale, under either hole or electron doping, in any simple way with J that should be approximately equivalent in the two types of materials. Combined with the new experimental data, the calculations indicate the anomaly can be connected to a transition, or cross-over, from a quasi-particle band at low binding energy near E_f to the incoherent lower Hubbard band, or more precisely oxygen valence bands, at higher binding energy.

Qualitatively, the doping and momentum dependence obtained from calculations are similar to the experimental results and, in many cases, minor adjustments to model parameters produce even surprisingly close quantitative agreement with the observed features [2, 3, 4, 5, 6, 7, 8, 9], especially those presented here on electron-doped NCCO. However, the single-band Hubbard model should only be viewed as a low energy effective model of the cuprates. A better understanding of the role played

by strong correlations would come from careful analysis of calculations explicitly incorporating planar oxygen states that would capture the formation of Zhang-Rice singlets [21] and the spectral weight associated with the valence bands, assumed to have strong oxygen character.

The authors would like to thank R. Hackl, M. Jarrell, W. S. Lee, A. Macridin, T. Maier and F. Vernay for valuable discussions. The authors acknowledge support from DOE DE-FG03-01ER45929-A001, DOE DE-FC02-06ER25793 (SciDac), DOE DE-AC02-76SF00515, NSF DMR-0705086 and NSERC. This work was made possible, in part, by computational support from the National Energy Research Scientific Computing Center under DOE Contract No. DE-AC02-05CH11231, NSF through TeraGrid resources provided by the National Center for Supercomputing Applications, Réseau Québécois de Calcul de Haute Performance through Mammouth-parallèle at the University of Sherbrooke and the facilities of SHARCNET. Three of the authors (BM, SJ, TPD) wish to thank the Walther Meißner Institute and the Pacific Institute of Theoretical Physics for their hospitality during part of this work.

-
- [1] A. Damascelli *et al.*, Rev. Mod. Phys. **75**, 473 (2003).
 - [2] W. Meevasana *et al.*, Phys. Rev. B **75**, 174506 (2007).
 - [3] J. Graf *et al.*, Phys. Rev. Lett. **98**, 067004 (2007).
 - [4] B. P. Xie *et al.*, Phys. Rev. Lett. **98**, 147001 (2007).
 - [5] J. Chang *et al.*, Phys. Rev. B **75** (2007).
 - [6] T. Valla *et al.*, Phys. Rev. Lett. **98**, 167003 (2007).
 - [7] D. S. Inosov *et al.*, Phys. Rev. Lett. **99**, 237002 (2007).
 - [8] Z.-H. Pan *et al.*, arXiv:cond-mat/0610442 (2006).
 - [9] W. Zhang *et al.*, arXiv:0801.2824v1 (2008).
 - [10] F. Ronning *et al.*, Phys. Rev. B **71**, 094518 (2005).
 - [11] E. Manousakis, Phys. Rev. B **75**, 035106 (2007).
 - [12] A. S. Alexandrov and K. Reynolds, Phys. Rev. B **76**, 132506 (2007).
 - [13] A. Macridin *et al.*, Phys. Rev. Lett. **99**, 237001 (2007).
 - [14] R. S. Markiewicz *et al.*, Phys. Rev. B **76**, 174514 (2007).
 - [15] R. S. Markiewicz and A. Bansil, Phys. Rev. B **75**, 020508 (2007).
 - [16] K. Byczuk *et al.*, Nature Phys. **3**, 168 (2007).
 - [17] F. Tan *et al.*, Phys. Rev. B **76**, 054505 (2007).
 - [18] M. M. Zemljic *et al.*, Phys. Rev. Lett. **100**, 036402 (2008).
 - [19] C. Weber *et al.*, arXiv:cond-mat/0804.1512 (2008).
 - [20] W. Meevasana *et al.*, Phys. Rev. B **77**, 104506 (2008).
 - [21] F. C. Zhang and T. M. Rice, Phys. Rev. B **37**, 3759 (1988).
 - [22] P. W. Anderson, Science **235**, 1196 (1987).
 - [23] S. R. White *et al.*, Phys. Rev. B **40**, 506 (1989).
 - [24] R. Blankenbecler *et al.*, Phys. Rev. D **24**, 2278 (1981).
 - [25] M. Jarrell and J. Gubernatis, Phys. Rep. **269**, 133 (1996).
 - [26] A. Macridin *et al.*, arXiv:cond-mat/0410098v1 (2004).
 - [27] H. Eskes *et al.*, Phys. Rev. Lett. **67**, 1035 (1991).
 - [28] P. G. Steeneken *et al.*, Phys. Rev. Lett. **90**, 247005 (2003).
 - [29] R. Preuss *et al.*, Phys. Rev. Lett. **75**, 1344 (1995).
 - [30] Q. Yin *et al.*, Phys. Rev. Lett. **100**, 066406 (2008).

- [31] C. Gröber *et al.*, Phys. Rev. B **62**, 4336 (2000).
- [32] E. Dagotto, Rev. Mod. Phys. **66**, 763 (1994).